IOPscience iopscience.iop.org

Home Search Collections Journals About Contact us My IOPscience

Study of a pulsed capillary discharge waveguide with a modulated radius

This article has been downloaded from IOPscience. Please scroll down to see the full text article.

2006 J. Phys. D: Appl. Phys. 39 2384

(http://iopscience.iop.org/0022-3727/39/11/012)

View the table of contents for this issue, or go to the journal homepage for more

Download details:
IP Address: 130.89.112.124
The article was downloaded on 09/04/2013 at 10:38

Please note that terms and conditions apply.

INSTITUTE OF PHYSICS PUBLISHING JOURNAL OF PHYSICS D: APPLIED PHYSICS

J. Phys. D: Appl. Phys. **39** (2006) 2384–2390 doi:10.1088/0022-3727/39/11/012

Study of a pulsed capillary discharge waveguide with a modulated radius

B H P Broks[1], J van Dijk[1], H M J Bastiaens[2], K J Boller[2] and J J A M van der Mullen[1]

[1] Department of Applied Physics, Eindhoven University of Technology, PO Box 513, 5600 MD Eindhoven, The Netherlands
[2] Department of Science and Technology, University of Twente, PO Box 217, 7500 AE Enschede, The Netherlands

E-mail: j.j.a.m.v.d.mullen@tue.nl

Received 16 March 2006, in final form 17 March 2006
Published 18 May 2006
Online at stacks.iop.org/JPhysD/39/2384

Abstract
Slow pulsed capillary discharges are under investigation for use as plasma channel waveguides in laser-wakefield acceleration and high-harmonics generation. The channel radius has a strong influence on the plasma and guiding properties. Hence, it is expected that the guiding properties can be manipulated by locally modifying the radius. This presumption has been investigated by means of a numerical simulation of a channel with a periodically modulated radius. The simulation revealed a strongly nonlinear response of the plasma and wall properties to the modulation. However, no modulation of the laser guiding properties is observed.

(Some figures in this article are in colour only in the electronic version)

1. Introduction

The interaction between compact, high-powered femtosecond lasers [1] and plasmas gives rise to many interesting physical phenomena, such as high-harmonic generation [2, 3], x-ray lasing [4–7] and laser-wakefield acceleration [8–10]. In all these cases, the interaction length between laser and plasma is of critical importance. This interaction length can be increased to many times the Rayleigh length by means of optical laser guiding [11, 12]. This can be achieved using a plasma waveguide with a convex, parabolic refractive index pattern.

Such waveguides can be generated in wall-ablating capillary discharges [13–17], in pinch plasmas [18–20] and in slow capillary discharges [21–24]. Our investigation focuses on the latter, which have the advantages of long lifetime and stability.

A slow capillary discharge waveguide consists of a straight capillary made of a material resistant to short, intense thermal loads, such as alumina or quartz. This capillary is filled with a gas that is easily fully ionized, such as helium or hydrogen, with a pressure that is typically between 10^2 and 10^4 Pa. A current pulse of a few hundred amperes that lasts for a few hundred nanoseconds is then sent through the discharge. This current pulse causes nearly full ionization of the plasma. However, mainly due to the short duration, ablation of wall material may be avoided, which allows the waveguide to be used many times.

The pulsed capillary discharge waveguide has been analysed both experimentally [22, 23] and numerically [21,24–26]. In this work, we focus on an expansion of this analysis by numerically modelling capillary discharge waveguides with a periodically modulated radius. This is of great interest for the following reasons.

- A real waveguide is not perfectly straight and smooth. By investigating the effect of wall irregularities, insight into the robustness of the laser guiding and plasma properties with respect to these irregularities can be gained.
- A periodic variation of the radius might impose a periodic variation in the plasma properties density. It is known that for a straight channel the matched laser spot size and hence the intensity depends strongly on the channel radius [21, 27]. Hence, it might be expected that a periodic variation of the channel radius can be used to modulate the laser intensity along the axis of the channel. This approach might have potential applications in high-harmonic generation, where a strong enhancement of the conversion efficiency is observed when waveguides

 © 2006 IOP Publishing Ltd Printed in the UK

with a modulated radius are used instead of straight waveguides [28].

- Using a tapered channel [29] might lead to a variation in axial density. This can be used to keep the laser and electron bunch in phase over a longer distance in laser-wakefield acceleration. Modelling channels with a varying radius will be useful in predicting the properties of tapered channels.
- By applying a longitudinal structure, the problem is no longer essentially one-dimensional. This allows for an analysis of the relative importance of longitudinal and radial transport in the plasma.

Discharge capillaries with a well-defined periodic structure are much more difficult to manufacture than straight capillaries. Hence, numerical modelling, especially using a method that is experimentally validated [24], is particularly suitable for an investigation of the conditions required to generate modulated plasma waveguides.

In section 2 of this paper, we start by pointing out the requirements for laser guiding in a plasma channel. The discharge capillaries in which the waveguides are generated will be described in detail in section 3. The model used to simulate the plasma waveguides is discussed in section 4. The results obtained from the numerical simulations are presented in section 5, with an emphasis on the laser-guiding properties of the waveguide and the heating of the capillary wall. Conclusions are presented in section 6.

2. Laser guiding

For the guiding of laser beams, a convex index of refraction pattern is needed [30]. A suitable profile for the guiding of Gaussian laser beams is formed by a concave, parabolic electron density n_e profile, such as given by

$$n_e(r) = a + \frac{1}{2}br^2, \tag{1}$$

where a is the on-axis density, b the second derivative of n_e and r is the radial coordinate. The matched spot W_m for a laser in this density profile is given by [21]

$$W_m = (0.5\pi r_e b)^{-1/4}, \tag{2}$$

with r_e the classical electron radius, which is given by

$$r_e = \frac{e^2}{4\pi\epsilon_0 m_e c^2}, \tag{3}$$

where e is the charge of the electron, ϵ_0 the permittivity of vacuum, m_e the electron mass and c the speed of light. Equation (3) shows that r_e has a numerical value of 2.817×10^{-15} m. The matched spot size of a simulated plasma channel can be obtained by fitting the central electron density profile with equation (1) and substituting the obtained b-value in equation (2). The electron density profile needs to be concave and (approximately) parabolic only near the centre of the discharge, for a radius of about 1.5 W_m, for the bulk of the laser power to be transmitted as a Gaussian pulse.

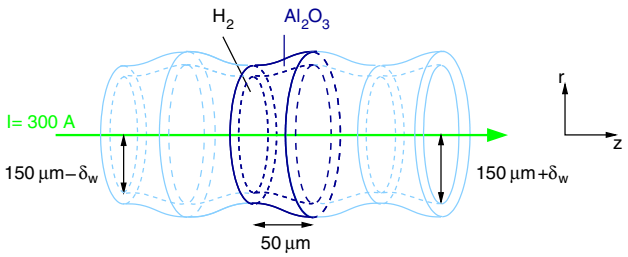

Figure 1. The discharge capillary with a modulated inner radius. The modelled system is indicated in bold, and is assumed to be part of an infinitely long capillary. The parameter δ_w is the amplitude of the radius modulation, while the average capillary radius is 150 μm. The periodicity of the modulation is 100 μm.

3. The discharge capillary

For this study, we remain as close as possible to an actually existing system, namely the capillary waveguide described by Spence and Hooker [31]. This waveguide has been the subject of earlier numerical studies [21, 24], making it a good starting point for this study.

This waveguide is generated in a cylinder-symmetric alumina capillary with a radius r_0 of 150 μm, which is filled with 67 mbar of hydrogen and subjected to one half-cycle of a sinusoidal current pulse with a half-time of 200 ns and an amplitude of 300 A. The plasma thus produced will heat the wall, liberating adsorbed hydrogen. This contribution is estimated in [24] and brings the total hydrogen density to 2.16×10^{24} m^{-3}.

In this study, the capillary is modified by periodically varying the radius r_c with a modulation amplitude δ_w:

$$r_c = r_0 + \delta_w \sin\left(\frac{2\pi z}{z_{mod}}\right), \tag{4}$$

where z is the axial coordinate. In this study, we restrict ourselves to a modulation period of z_{mod} of 100 μm, which is of the same order of magnitude as the channel radius. Modulation lengths that are much longer than the capillary radius will most likely preclude the formation of a stable channel because the longitudinal bulk transport time becomes comparable to the current pulse length.

The system as modelled is shown in figure 1. Owing to the periodicity of the system, only one-half of one modulation period needs to be treated. The system will be treated for $\delta_w = 25\,\mu$m, which is a significant amplitude resulting in a modulation in plasma area of almost a factor 2, and for $\delta_w = 5\,\mu$m, which is a much smaller amplitude that is more representative for surface roughness. For relevant cases, these results will be compared with the results for the null case $\delta_w = 0\,\mu$m, which are given in [24].

4. Model of the plasma waveguide

The discharge capillary waveguide has been modelled in [24] using the PLASIMO code [32–37], with a good match between theoretical and experimental results. We use this model as a basis for the modelling in this work. Because the model is described in detail in [24], the discussion will be restricted to a brief summary and a discussion of the new aspects of the

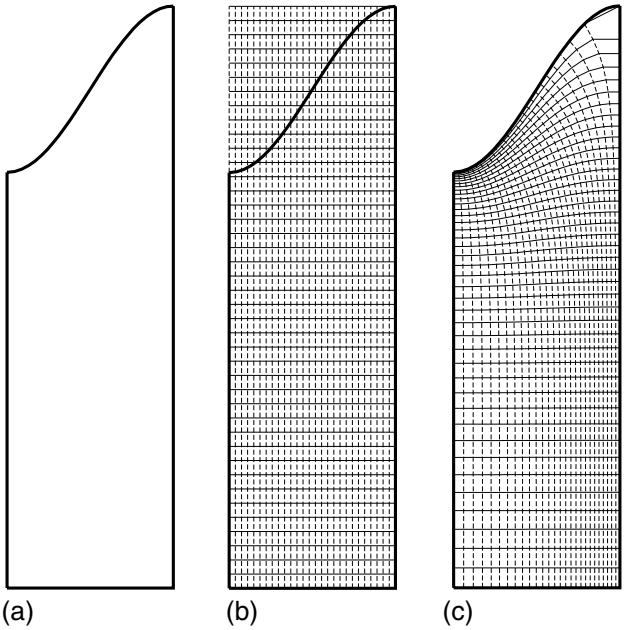

Figure 2. The geometry of an object with a curved boundary (*a*) can be approximated as a slice of a rectangular grid (*b*). Alternatively, a boundary-fitted OCL grid may be employed (*c*).

current model that is used to treat the periodic modulation of the radius; the interested reader is referred to [24] for details.

The pulsed capillary discharge waveguide basically consists of a plasma contained in a capillary. For an accurate treatment, two different regions have to be simulated: the plasma and the temperature evolution of the wall material. These two aspects are modelled separately and coupled using the boundary conditions.

The basis of the plasma model is formed by a time-dependent two-dimensional non-LTE quasi-neutral fluid model, which is used extensively in the description of low-temperature plasmas and has a wide range of validity. In this approach, it is assumed that the electrons have a temperature T_e and the heavy particles have a temperature T_h, which may differ. The Navier–Stokes equations are solved to describe the bulk flow, which reaches significant Mach numbers. The non-LTE approach allows for deviations from chemical equilibrium, and the densities of four separate species, namely e, H^+, H and H_2, are modelled. These differences from chemical equilibrium were found to be important in the formation of the channel [24].

The difference in the earlier simulations [24–26] is the non-uniform channel radius. In order to model the longitudinal variation of the radius of the capillary we have made use of the fact that the discretization code in the PLASIMO framework has been expressed in general ortho-curvilinear (OCL) coordinates. Such coordinates allow for a boundary-fitted grid, as suggested in figure 2(*c*). The advantages with respect to the 'slicing' method in figure 2(*b*) are twofold.

- The boundary conditions can be easily specified in terms of the single coordinate perpendicular to the boundary.
- Since all grid points are part of the region of interest, this region can be mapped to a structured (orthonormal) *computational* mesh.

The mapping between the computational and physical coordinate intervals are given by a metric tensor which—in view of the (local) orthogonality—contains diagonal elements only.

The implementation of the grid generation module in PLASIMO is based on the method of elliptic partial differential equations as discussed by Mobley and Stewart [38]. An advantage of this method is that the grid does not need to be isometric, as in the earlier work of Pope [39]: by specifying appropriate *stretch functions* the grid line density in each of the coordinate directions can be tuned. As a result one can increase the grid line density in regions where large gradients are expected. The implementation of this method in PLASIMO is described in detail in [32, 33].

For the wall, the temperature equation is numerically solved on a two-dimensional grid that describes the innermost 5 μm of the wall. The temperature-dependent thermal conductivity [40–42] and heat capacity [40, 43] of polycrystalline alumina are used. The melting and ablation of alumina, which has a melting point of about 2300 K [40], is not included in the model. Coupling of the plasma–wall interface is achieved by matching the T_h in the plasma with the wall temperature T_w while matching the heat flux out of the plasma with the heat flux into the wall. This implies that the electron temperature T_e is not coupled to the wall temperature. The coupling is underrelaxed to improve stability. Note that the very shallow penetration of the wall heating, much less than the 5 μm simulated, requires a very fine grid to be described correctly. Hence, solving both the wall and the plasma on the same grid will lead to unacceptably large discretization errors or excessive computation times.

5. Results and discussion

The pulsed capillary discharge waveguides with a periodically modulated radius has been modelled for two values of δ_w, namely $\delta_w = 25\ \mu$m and $\delta_w = 5\ \mu$m. First, the formation of a stable channel is discussed. Next, the laser guiding properties at the peak of the current ($t = 100$ ns) are discussed based on the n_e-profiles. Finally, the heating of the wall is discussed.

Initially, the plasma has a low degree of ionization and is at rest. The current passing through the plasma heats the electrons, causing ionization. The Ohmic dissipation varies with r_c^{-4} in first order, as it is proportional to the current density J^2, while J is proportional to r_c^{-2} [25, 26]. Hence, the narrow parts of the channel ionize much faster than the broader parts, as can be seen in figure 3, which shows n_e as a function of z and r at $t = 15$ ns, for the channel with $\delta_w = 25\ \mu$m.

The pressure near the axis of the discharge increases due to heating, in particular in the narrow parts, as is shown in figure 3. This pushes the plasma to the broader, colder parts of the channel, especially to the cooler walls. This creates a concave plasma bulk density profile. The plasma temperature becomes so high that the plasma is nearly fully ionized, except near the walls, resulting in a concave electron density profile. The high electron density and resulting frequent electron/heavy particle collisions make the electron temperature T_e and the heavy particle temperature T_h nearly equal over the central part of the discharge [24]. The formation of such a stable profile takes about 70 ns. For the values of δ_w under study,

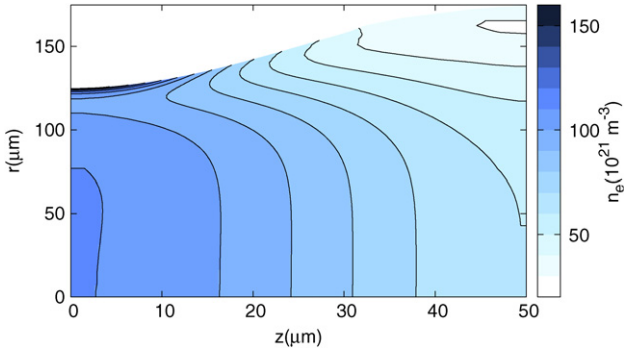

Figure 3. The electron density in the pulsed capillary discharge at $t = 15$ ns. In the narrowest part the electron density is almost a factor of 2 higher than the electron density in the broadest part.

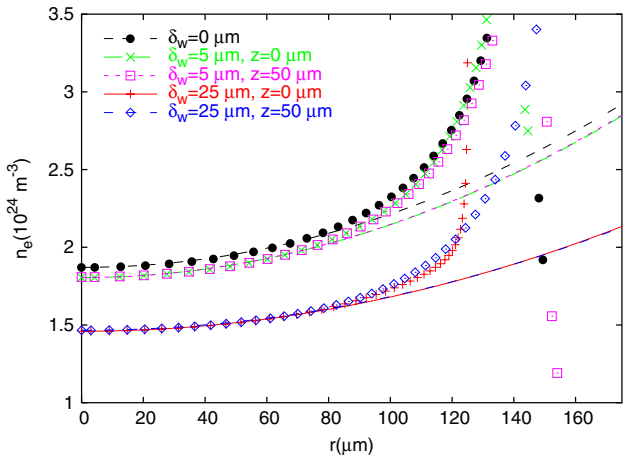

Figure 4. The electron density in the pulsed capillary discharge at $t = 100$ ns, for various values of δ_w at the narrowest ($z = 0\,\mu$m) and broadest ($z = 50\,\mu$m) part of the channel. Note that the ordinate has a restricted range, in order to emphasize the central part of the discharge. Some data points near the wall are therefore not displayed. The central density profile is almost independent of z, but does depend on δ_w.

the electron density profiles at the narrowest and the broadest part of the discharge, evaluated at $t = 100$ ns, are presented in figure 4.

Figure 4 clearly shows two trends. Firstly, there is almost no difference in the central electron density profile between the narrowest and the broadest part of the discharge. Because the matched spot size W_m depends solely on the central electron density profile (cf (1) and (2)), the laser beam will not be modulated by the channel wall modulation. Because it is known that the guiding of the laser beam depends strongly on channel radius for unmodulated channels [21, 25, 26], this is an unexpected result that deserves closer inspection.

As mentioned, the central electron density profile is formed by temperature differences in the channel, with the hottest parts of the plasma having the lowest density. For $\delta_w = 25\,\mu$m and $t = 100$ ns, T_e as a function of r and z is depicted in figure 5. The electron temperature in the centre of the channel is high. This means that the thermal conductivity λ_e, which scales as $\lambda_e \propto T_e^2$, is much higher in the centre of the channel than near the walls. Hence, axial heat transport becomes much faster than radial heat transport. The fast axial

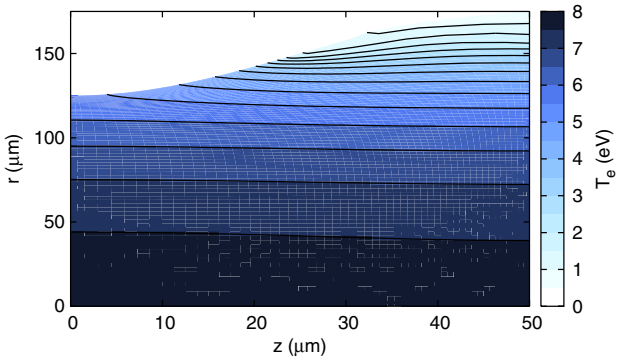

Figure 5. The electron temperature in the pulsed capillary discharge for δ_w at $t = 100$ ns. The temperature in the central part of the discharge is almost independent of z.

Table 1. The a and b parameters and the matched spot size W_m for three capillaries, at different axial positions.

δ_w (μm)	z(μm)	a (10^{24} m^{-3})	b (10^{31}m^{-5})	W_m (μm)
0	0	1.87	6.86	42.6
5	0	1.81	6.79	42.7
5	50	1.81	6.83	42.7
25	0	1.46	4.4	47.6
25	50	1.47	4.3	47.8

transport leads to a central temperature profile that is nearly independent of z; hence, the central electron density profile is nearly independent of z as well.

The second trend that is visible in figure 4 is that the central density is lower for channels that have a higher δ_w. When r_c is modulated, the broader parts of the channel are further from the central channel, leading to lower temperatures. These low-temperature areas acts as sinks for hydrogen, particularly because the temperature becomes so low in these areas that the plasma has only a modest degree of ionization.

In figure 4, fits of the central electron density to a parabola (cf equation (4)) are presented. The resulting a and b and W_m obtained using equation (2) are presented in table 1. For all the cases, the area over which the channel is approximately parabolic is significantly larger than the matched spot size, permitting the guiding of Gaussian laser pulses.

For $\delta_w = 25\,\mu$m, the matched spot size is larger than for the other cases. This is mainly due to lower plasma density in the centre of the channel. The lower density reduces b, reducing the focusing power of the plasma and increasing the matched spot size.

Having investigated the influence that the radius modulation has on the plasma and guiding properties, we will now consider the influence it has on the capillary wall. The wall is heated by the plasma, and the highest temperatures during the discharge are reached at the plasma–wall interface. The temperature at the plasma–wall interface T_{pw} as a function of z and t is displayed for the channel with $\delta_w = 5\,\mu$m in figure 6.

Figure 6 shows that the temperature distribution becomes strongly peaked as the discharge progresses in time, with the highest temperatures in the narrowest part of the discharge, even for a small modulation of the channel radius. The dissipation is higher in the narrower parts of the channel. However, because the radius modulation is only 3%, this effect

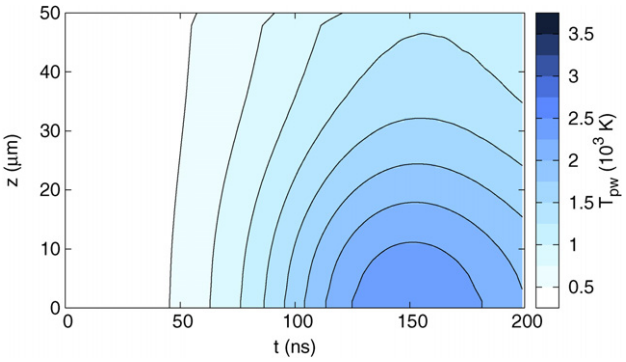

Figure 6. The temperature at the plasma–wall interface, for $\delta_w = 5\,\mu$m, as a function of z and t. The temperature starts out relatively uniform but becomes strongly peaked near the narrow part of the channel ($z = 0$) as the discharge progresses in time. The temperature slightly exceeds the melting temperature of alumina (2300 K [40]) at this peak.

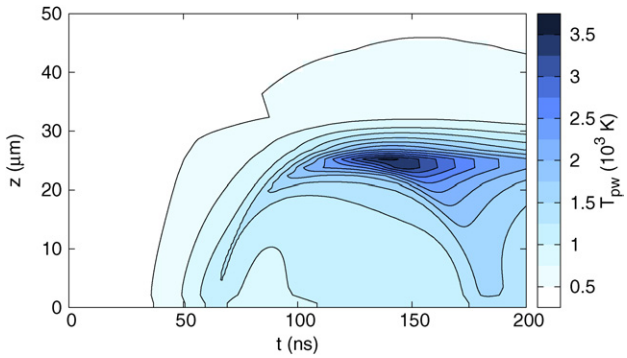

Figure 7. The temperature at the plasma–wall interface, for $\delta_w = 25\,\mu$m, as a function of z and t. The temperature starts out relatively uniform, but becomes strongly peaked at the narrowest point of the discharge. This temperature peak then travels over the plasma–wall interface.

is too small to fully account for the observed peaking. There are two other effects that cause the temperature to peak.

After about 45 ns, the plasma is somewhat hotter in the narrow parts of the discharge. This leads to an increase in thermal conductivity and increases the heat flux to the wall. The good thermal contact between this plasma area at the wall and the hotter central plasma allows for most of the heat to flow trough this plasma area. The high thermal conductivity of the hot central plasma allows for fast axial heat transport. This allows the heat flux to bypass the cooler plasma areas, where the plasma cannot sustain a large heat flux to the wall.

The transport properties of the wall respond to a change in temperature as well. In particular, the thermal conductivity of a solid is inversely proportional to its temperature [41, 42]. This causes the wall to lose its heat more slowly when it gets hotter, thus amplifying temperature differences.

The wall reaches a temperature that is above the melting point of alumina (Al_2O_3). This may lead to erosion of the narrow parts of the channel. Furthermore, the plasma might be contaminated with wall material. Because aluminium and oxygen are not fully ionized at the temperatures that are reached in the plasma, this may lead to undesired ionization-induced defocusing [44]. Because the effect of ablation is not included in the model, the quantitative significance of the results is reduced from the moment ablation first occurs (for $t > 128$ ns).

For $\delta_w = 25\,\mu$m, the behaviour of the wall temperature is more complex, as can be seen in figure 7. The wall is initially hottest at the narrowest part of the discharge, for reasons explained above. After this, the hottest part of the wall moves along the surface.

As mentioned in section 4, the electrons do not transfer their heat directly to the wall, but rather transfer their heat to the heavy particles by elastic collisions, and these heavy particles transfer their heat to the wall. The elastic energy transfer rate P_{elEH} between electrons and heavy particles can be approximated well by the transfer rate for a fully ionized plasma $P^{\mathrm{fi}}_{\mathrm{elEH}}$ for the times and regions of interest. $P^{\mathrm{fi}}_{\mathrm{elEH}}$ is given by the product of the energy transferred per collision E_{coll} and the collision frequency ν_{ei} (5) [45]:

$$P_{\mathrm{elEH}} \approx P^{\mathrm{fi}}_{\mathrm{elEH}} = E_{\mathrm{coll}}\nu_{ei}. \tag{5}$$

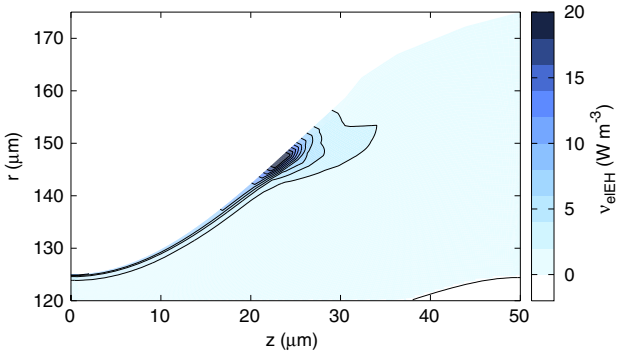

Figure 8. The electron-heavy particle elastic energy transfer rate, for $\delta_w = 25\,\mu$m at $t = 100$ ns, as a function of r and z. Only the plasma close to the wall, where this transfer rate is highest, is shown. The transfer rate is strongly peaked and highest halfway between the narrowest and the broadest part of the channel.

Here, E_{coll} is given by

$$E_{\mathrm{coll}} = 2\frac{m_e}{m_{H^+}}\frac{3}{2}k_B\,(T_e - T_h)\,. \tag{6}$$

Here, m_{H^+} is the H^+ mass and k_B is Boltzmann's constant. ν_{ei} is given by

$$\nu_{ei} = n_e n_{H^+}\frac{4\sqrt{2\pi}}{3}\left(\frac{m_e}{k_B T_e}\right)^{3/2}\left(\frac{e^2}{4\pi\epsilon_0 m_e}\right)\ln\Lambda\,. \tag{7}$$

Here, n_{H^+} is the H^+ density and $\ln\Lambda$ is the Coulomb logarithm, which is about 3 for this plasma. Equation (5) predicts a maximum in the electron energy transfer rate as a function of T_e, corresponding to the highest local heating of the wall. As can be seen in figure 5, the electron temperature near the wall is highest in the narrowest part of the channel and lowest near the broadest part. The highest ν_{elEH} is reached roughly at $z = 25\,\mu$m for $t = 100$ ns, as can be seen in figure 8.

Comparing the electron temperature T_e at the wall in figure 5 and the heavy particle temperature T_h at the wall in figure 7 shows that T_e is much higher than T_h in the narrow part of the channel. This difference can be ascribed to the decrease in P_{elEH} with increasing T_e, allowing for a local runaway of T_e. This clearly underscores the importance of a non-LTE treatment.

We see that the interaction between the plasma and the wall is complex and highly nonlinear, with both the temperature dependence of the wall properties and the deviations from thermal equilibrium playing an important role. However, the two-region model with under-relaxed coupling, as described in section 3, was sufficiently robust to handle the nonlinearities and the very different length and time-scales of the transport in the plasma and the wall, in a computational time that was quite managable (several days at most).

6. Conclusions

We have numerically modelled a pulsed capillary discharge waveguide with a sinusoidally modulated radius, using a two-region model with an under-relaxed coupling to efficiently treat the very different length and timescales of the transport in the capillary and in the plasma. Two general trends were observed.

Firstly, while the modulation does influence the plasma near the wall, the central plasma and hence the matched spot size is not significantly modulated, due to the fast axial heat transport, for the modulation depths under study. This means that the laser beam cannot be modulated by modulating the channel radius for the modulation depths under study and that modulation by surface roughness has no significant influence on the laser propagation either.

Secondly, the radius modulation causes a strongly nonuniform wall temperature, and temperatures above the melting temperature of alumina are reached. For a channel with a 5 μm radius modulation, the wall temperature is highest at the narrowest part of the channel. Ablation there will widen the channel and hence reduce the modulation. In practice, this means surface roughness may be ablated by the discharge, smoothening the channel. For a channel with a 25 μm radius modulation, the hottest part of the wall moves over the surface in time. In this case, significant ablation is expected.

From this, it is concluded that surface roughness does not influence the performance of the plasma waveguide. Furthermore, wall radius modulation is not expected to be a useful technique for tailoring the laser guiding properties of the waveguide.

Acknowledgments

The authors would like to thank A J Gonsalves for the fruitful discussions. The PLASIMO team members, current and former, are acknowledged for their contributions to the code. This work was performed as part of the research program of 'Stichting voor Fundamenteel Onderzoek der Materie' (FOM) with financial support from NWO, within the FOM program 55 on Laser Wakefield Accelerators.

References

[1] Perry M D and Mourou G 1994 Terawatt to petawatt subpicosecond lasers *Science* **264** 917–24

[2] Milchberg H M, III Durfee C G and McIlrath T J 1995 High-order frequency conversion in the plasma waveguide *Phys. Rev. Lett.* **75** 2494–7

[3] Tamaki Y, Itatani J, Nagata Y, Obara M and Midorikawa K 1999 Highly efficient, phase-matched high harmonic generation by a self-guided laser beam *Phys. Rev. Lett.* **82** 1422

[4] Butler A, Gonsalves A J, McKenna C M, Spence D J, Hooker S M, Sebban S, Mocek T, Bettabi I and Cros B 2002 Demonstration of a collisionally excited optical-field-ionization XUV laser driven in a plasma waveguide *Phys. Rev. Lett.* **91** 205001

[5] Butler A, Gonsalves A J, McKenna C M, Spence D J, Hooker S M, Sebban S, Mocek T, Bettabi I and Cros B 2004 A 41.8 nm Xe^{8+} laser driven in a plasma waveguide. *Phys. Rev.* A **70** 023821

[6] Lemoff B E, Yin G Y, Gordon C L III, Barty C P J and Harris S E 1995 Demonstration of a 10-hz femtosecond-pulse-driven XUV laser at 41.8 nm in Xe IX *Phys. Rev. Lett.* **74** 1574–7

[7] Korobkin D V, Nam C H, Suckewer S and Goltso A 1996 Demonstration of soft x-ray lasing to ground state in Li III *Phys. Rev. Lett.* **77** 5206–9

[8] Joshi C and Corkum P B 1995 Interactions of ultra-intense laser light with matter *Phys. Today* **48** 36

[9] Geddes C G R, Toth Cs, Van Tilborg J, Esarey E, Schroeder C B, Bruhwiler D, Nieter C, Cary J and Leemans W P 2004 High-quality electron beams from a laser wakefield accelerator using plasma-channel guiding. *Nature* **431** 538–41

[10] Mangles S P D *et al* 2004 High-quality electron beams from a laser wakefield accelerator using plasma-channel guiding *Nature* **431** 534–8

[11] Durfee C G III and Milchberg H M 1993 Light pipe for high intensity laser pulses *Phys. Rev. Lett.* **71** 2409–12

[12] Ehrlich Y, Cohen C, Kaganovich D, Zigler A, Hubbard R F, Sprangle P and Esarey E 1998 Guiding and damping of high-intensity laser pulses in long plasma channels *J. Opt. Soc. Am.* B **15** 2417

[13] Ehrlich Y, Cohen C, Zigler A, Krall J, Sprangle P and Esarey E 1996 Guiding of high-intensity laser pusles in straight and pulsed plasma experiments *Phys. Rev. Lett.* **77** 4186

[14] Kaganovich D, Ting A, Moore C I, Zigler A, Burris H R, Ehrlich Y, Hubbard R and Sprangle P 1999 High efficiency guiding of terawatt laser pulses in a capillary discharge plasma channel *Phys. Rev.* E **59** R4769

[15] Hooker S M, Spence D J and Smith R A 2000 Guiding of high-intensity laser pulses in a discharge-ablated capillary waveguide *J. Opt. Soc. Am.* B **17** 90

[16] Marconi M C, Moreno C H, Rocca J J, Shlyaptsev V N and Osterheld A L 2000 Dynamics of a microcapillary discharge using a soft x-ray laser backlighter *Phys. Rev.* E **62** 7209

[17] Li B and Kwok D Y 2004 Multi-dimensional process for a pulse ablating capillary discharge: modeling and experiment *J. Plasma Phys.* **70** 397

[18] Hosokai T, Kando M, Dewa H, Kotaki H, Kondo S, Hasegawa N, Nakajima K and Horioka K 2000 Optical guidance of terrawatt laser pulses by the implosion phase of a fast Z-pinch discharge in a gas-filled capillary *Opt. Lett.* **25** 10–12

[19] Fauser C and Langhoff H 2000 Focussing of laser beams by means of a z-pinch formed plasma guiding system. *Appl. Phys. B: Lasers Opt.* **71** 607

[20] Hayashi Y, Sakamoto N, Zhao Y, Cheng Y, Chalise P, Watanabe M, Okino A, Horioka K and Hotta E 2004 On the time of lasing onset and the end-effect of a soft x-ray laser device using a capillary z-pinch discharge *Plasma Sources Sci. Technol.* **15** 675

[21] Bobrova N A, Esaulov A A, Sakai J I, Sasorov P V, Spence D J, Butler A, Hooker S M and Bulanov S V 2002 Simulations of a hydrogen-filled capillary discharge waveguide *Phys. Rev.* E **65** 016407

[22] Butler A, Spence D J and Hooker S M 2002 Guiding of high-intensity laser pulses with a hydrogen-filled capillary discharge waveguide *Phys. Rev. Lett.* **89** 195003

[23] Spence D J, Butler A and Hooker S M 2003 Gas-filled capillary discharge waveguides *J. Opt. Soc. Am.* B **20** 138

[24] Broks B H P, Garloff K and Van der Mullen J J A M 2005 A nonlocal-thermal-equilibrium model of a pulsed capillary discharge waveguide *Phys. Rev.* E **71** 16401
[25] Broks B H P, Van Dijk W and Van der Mullen J J A M 2005 Influence of the channel radius in a pulsed capillary discharge *Proc. XXVII ICPIG (Eindhoven)*
[26] Broks B H P, Van Dijk W and Van der Mullen J J A M 2006 Parameter study of the plasma and optical guiding properties of a pulsed capillary discharge waveguide *J. Phys. D: Appl. Phys.* **39** 2377
[27] Broks B H P, Van Dijk W and Van der Mullen J J A M 2005 Study of a pulsed capillary discharge with a modulated radius *Proc. XXVII ICPIG (Eindhoven)*
[28] Gibson E A, Zhang X, Popmintchev T, Paul A, Wagner M, Lytle A, Christov I P, Murnane M M and Kapteyn H C 2004 Extreme nonlinear optics: attosecond photonics at short wavelengths *IEEE J. Sel. Top. Quantum. Electron.* **10** 1339–50
[29] Sprangle P, Esarey E, Krall J and Joyce G 1992 Propagation and guiding of intense laser pulses in plasmas *Phys. Rev. Lett.* **69** 2200–3
[30] Esarey E, Sprangle P, Krall J and Ting A 1996 Overview of plasma-based accelerator concepts *IEEE Trans. Plasma. Sci.* **24** 252
[31] Spence D J and Hooker S M 2001 Investigation of a hydrogen plasma waveguide *Phys. Rev.* E **63** 015401(R)
[32] Benoy D A 1993 Modeling of argon plasmas *PhD Thesis* Eindhoven University of Technology
[33] Van Dijk J 2001 Modelling of plasma light sources *PhD Thesis* Eindhoven University of Technology
[34] Janssen G M 2000 Design of a general plasma simulation model, fundamental aspects and applications *PhD Thesis* Eindhoven University of Technology
[35] Van der Heijden H 2002 Modelling of radiative transfer in light sources *PhD Thesis* Eindhoven University of Technology
[36] Hartgers A 2003 Modelling of a fluorescent lamp plasma *PhD Thesis* Eindhoven University of Technology
[37] http://plasimo.phys.tue.nl/
[38] Mobley C D and Stewart J R 1980 On the numerical generation of boundary-fitted orthogonal curvilinear coordinate systems *J. Comput. Phys.* **34** 124–35
[39] Pope S B 1978 The calculation of turbulent recirculating flows in general orthogonal coordinates *J. Comput. Phys.* **26** 197–217
[40] Lide D R (ed) 2004 *CRC Handbook of Chemistry and Phyiscs* (Boca Raton, FL: CRC Press)
[41] Kittel C 1996 *Introduction to Solid State Physics* (New York: Wiley)
[42] Ziman J M 1960 *Electrons and Phonons* (Oxford: Oxford University Press)
[43] Atkins P W 1998 *Physical Chemistry* (Oxford: Oxford University Press)
[44] Rae S C 1993 Ionization induced defocusing of intense laser pulses in high-pressure gases *Opt. Commun.* **97** 25–8
[45] Mitchner M and Kruger C H 1983 *Partially Ionized Gasses* (New York: Wiley)